THE JOURNAL OF PHYSICAL CHEMISTRY A

Article

pubs.acs.org/JPCA

Structures of the Dehydrogenation Products of Methane Activation by 5d Transition Metal Cations

V. J. F. Lapoutre,[†] B. Redlich,[‡] A. F. G. van der Meer,[‡] J. Oomens,[‡,§] J. M. Bakker,*[,‡] A. Sweeney,[∥] A. Mookherjee,[∥] and P. B. Armentrout*[,∥]

[†]FOM Institute for Plasma Physics Rijnhuizen, Edisonbaan 14, 3439 MN Nieuwegein, The Netherlands

[‡]Institute for Molecules and Materials, Radboud University Nijmegen, FELIX Facility, Toernooiveld 7, 6525 ED Nijmegen, The Netherlands

[§]Van't Hoff Institute for Molecular Sciences, University of Amsterdam, Science Park 904, 1098 XH Amsterdam, The Netherlands

[∥]Department of Chemistry, University of Utah, 315 South 1400 East, Room 2020, Salt Lake City, Utah 84112, United States

Supporting Information

ABSTRACT: The activation of methane by gas-phase transition metal cations (M^+) has been studied extensively, both experimentally and using density functional theory (DFT). Methane is exothermically dehydrogenated by several 5d metal ions to form $[M,C,2H]^+$ and H_2. However, the structure of the dehydrogenation product has not been established unambiguously. Two types of structures have been considered: a carbene structure where an intact CH_2 fragment is bound to the metal (M^+-CH_2) and a carbyne (hydrido-methylidyne) structure with both a CH and a hydrogen bound to the metal separately (H-M^+-CH). For metal ions with empty d-orbitals, an agostic interaction can occur that could influence the competition between carbene and carbyne structures. In this work, the gas phase $[M,C,2H]^+$ (M = Ta, W, Ir, Pt) products are investigated by infrared multiple-photon dissociation (IR-MPD) spectroscopy using the Free-Electron Laser for IntraCavity Experiments (FELICE). Metal cations are formed in a laser ablation source and react with methane pulsed into a reaction channel downstream. IR-MPD spectra of the $[M,C,2H]^+$ species are measured in the 300−3500 cm^{-1} spectral range by monitoring the loss of H (2H in the case of $[Ir,C,2H]^+$). For each system, the experimental spectrum closely resembles the calculated spectrum of the lowest energy structure calculated using DFT: for Pt, a classic C_{2v} carbene structure; for Ta and W, carbene structures that are distorted by agostic interactions; and a carbyne structure for the Ir complex. The Ir carbyne structure was not considered previously. To obtain this agreement, the calculated harmonic frequencies are scaled with a scaling factor of 0.939, which is fairly low and can be attributed to the strong redshift induced by the IR multiple-photon excitation process of these small molecules. These four-atomic species are among the smallest systems studied by IR-FEL based IR-MPD spectroscopy, and their spectra demonstrate the power of IR spectroscopy in resolving long-standing chemical questions.

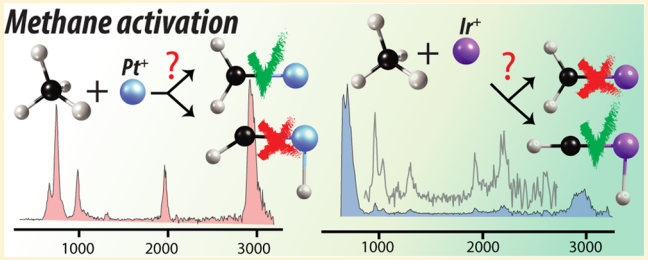

INTRODUCTION

Methane is an abundant feedstock and, via the Fischer−Tropsch process, it can be converted into liquid fuels or other products which are of interest because of their functionalized groups.[1] However, the production of Gas-to-Liquid (GTL) synthetic fuels via the Fischer−Tropsch process requires an additional first step for the conversion of natural gas into synthesis gas.[2] This two-step process is cumbersome and a more direct route to transform methane into more precious chemicals would be advantageous. To achieve this, activation of the strong and localized C−H bond, for instance by coordination complexes, is required.[3]

Gas-phase transition metal (TM) ions are often used as a model system for the fundamental interactions between TMs and methane. Although most gas-phase TM cations do not react with methane at thermal energies, the 5d TMs Ta^+, W^+, Os^+, Ir^+, and Pt^+ have been shown to activate methane exothermically by dehydrogenation (loss of H_2).[4−7] The question of why these particular TM ions activate methane and others do not has spurred investigations searching for the reaction pathways. The reaction of Pt^+ with methane has attracted special attention because of its relevance for the Degussa process, where hydrogen cyanide is formed from methane and ammonia over a platinum catalyst.[8−11] Recent overviews of studies of methane activation by TM ions in the gas phase are given by Roithova and Schröder,[12a] and Schlangen and Schwarz.[12b]

Although detailed thermodynamic studies aimed at extracting relevant binding energies have yielded extensive information about reactivity and energetics,[13−16] experimental information on the precise geometry of the $[M,C,2H]^+$ species is not available. Investigations of the geometric structure have so far been based on

Received: January 10, 2013
Revised: April 15, 2013
Published: April 16, 2013

theoretical calculations alone. Two possible types of structures have been predicted. The first is a structure with the carbon atom of the CH_2 fragment bound with a double bond to the metal.[17] This geometry has C_{2v} symmetry and is here referred to as a carbene structure. A second possibility is a hydrido-methylidyne structure (here labeled carbyne for brevity), where the metal is inserted into one of the C−H bonds, forming a triple bond to C−H and a single bond to H.[17,18] For maximum stability of this geometric structure, the metal needs to be able to form four bonds to the ligands instead of only two bonds for the carbene structure.

In their extensive theoretical examination of the 5d $[M,C,2H]^+$ species, Irikura and Goddard considered the carbyne structure, explicitly calculating the relative energies for $[Ta,C,2H]^+$ carbene and carbyne structures.[17] Here, the carbyne structure is significantly higher in energy than the carbene. The authors discarded carbyne structures for the other 5d TMs based on the general arguments that they are unable to form four covalent bonds (La^+, Hf^+, Pt^+, Au^+) or have larger exchange energy losses (W^+, Re^+, Os^+, Ir^+). Simon et al.[18] revisited this issue and performed calculations on a carbyne structure for the $[W,C,2H]^+$ complex, finding that the doublet carbyne structure is very close in energy to a quartet carbene structure that is distorted from C_{2v} to a lower symmetry C_s structure. The distortion is a result of agostic interactions, which can occur between an empty metal d-orbital and one of the C−H bonds forming a two-electron bond on the three centers M, C, and H.[19−21] For the 5d TM cations in their ground electronic states, one expects *a priori* that distorted carbene structures are only possible for La^+, Hf^+, Ta^+, and W^+, as the metal needs to possess an empty valence orbital (of suitable symmetry) for agostic interactions.[22,23] It will be shown below that Ir^+ (and by analogy, Re^+ and Os^+ as well) can undergo a spin change, thereby rearranging the occupation of the d-electron system to empty one orbital. This implies that these metals can, in principle, also participate in an agostic interaction.

Over the past decade, the combination of IR Free-Electron Lasers (IR-FELs) with mass spectrometric detection techniques has allowed the structural characterization of a wide variety of molecules and ions of relevance to biological, astrophysical, and catalytic applications.[24−27] However, the use of IR multiple-photon dissociation (IR-MPD) spectroscopy using IR-FELs for smaller systems is expected to suffer from inefficient excitation. In the generally accepted picture of multiple-photon excitation,[28,29] the photons required to induce dissociation are not absorbed in one vibrational coordinate until the dissociation barrier is reached, because the vibrational anharmonicity causes the exciting laser frequency to run out of resonance after the absorption of one or a few photons. Instead, after absorption of a photon in the accepting vibrational coordinate, the photon's energy is rapidly redistributed over all the vibrational degrees of freedom through Intramolecular Vibrational Redistribution (IVR).[30,31] As the vibrational density of states grows rapidly with the number of constituent atoms, smaller systems may have IVR rates that are not sufficiently high to ensure efficient delocalization of vibrational excitation thus impeding the absorption of multiple IR photons and dissociation within the experimental time window.

In concert with these considerations, only one IR-MPD spectrum for systems consisting of four or fewer atoms has thus far been reported. Pivonka et al.[32] reported the dissociation of $BrHBr^-$ upon irradiation at 1558 cm^{-1}. However, this band was not reproduced in a messenger-atom spectrum.[33] For neutrals, IR-MPD of NH_3 has been demonstrated in a gas cell using a line-tunable CO_2 laser.[34,35] For these studies, peak powers of ≈10 GW/cm^2 were required, and it was hypothesized that rotational line broadening effects assist in keeping overlap between the anharmonic vibrational mode spacing and the exciting laser frequency.

In the present work, the IR-MPD spectra of the four-atom $[M,C,2H]^+$ products formed after activating methane by four 5d TMs (M = Ta, W, Ir, Pt) are presented. IR radiation provided by the Free-Electron Laser for IntraCavity Experiments (FELICE) is employed to overcome the anharmonicity bottleneck. FELICE can provide peak powers exceeding the 10 GW/cm^2 used for CO_2 laser driven IR-MPD of NH_3.[36] To interpret the spectra, DFT calculations are carried out aimed at finding the lowest energy structures for several spin states, as well as to find the structures of transition states linking the various minima. It will be shown that the combination of experimental IR-MPD spectra and DFT calculations allows for an unambiguous assignment of the geometric and electronic structure of the four different systems.

METHODS

Experiment. The IR-MPD spectroscopic experiments on $[M,C,2H]^+$ are performed using the molecular beam instrument on the first beamline of FELICE, described previously.[36,37] Metal cations are produced in a Smalley-type laser ablation source.[38−40] The second harmonic of a pulsed Nd:YAG laser (532 nm) is focused onto a rotating metal target (for Ta, W, and Ir, solid rods are employed; for Pt, a thin foil is spot-welded onto a stainless steel rod). A short helium pulse, injected with a pulsed valve (General Valve Series 9), collisionally cools the formed plasma in a channel (3 mm diameter, 60 mm long). Approximately 50 mm downstream from the point of ablation, a pulse of methane is introduced in the channel via a second pulsed valve, and the metal ions react with the methane. Typically 40−60% of the metal ions react with methane. At the end of the channel, the gas pulse expands into vacuum. The molecular beam is skimmed first by a 2 mm diameter skimmer and, after traveling through a differential vacuum, by a horizontal slit aperture (8 × 2 mm), both of which are electrically grounded. After the skimmers, the ion beam enters the intracavity region where it is crossed by the FELICE IR laser beam in the horizontal plane at an angle of 35°. FELICE produces IR radiation in the 100−3500 cm^{-1} spectral range, although for the current experiments only the 300−3500 cm^{-1} range is used. The radiation is near transform-limited, and the spectral width is set to approximately 0.4% fwhm of the central frequency. FELICE laser pulses are produced in a pulse train, the so-called macropulse, with a typical duration of 5 μs, consisting of ps-long micropulses at a 1 ns separation.

A few μs after interaction with FELICE, all ions are pulse-extracted into a reflectron time-of-flight (RETOF) mass spectrometer (Jordan TOF Products, Inc.), with a typical mass resolution of $M/\Delta M \approx 1700$. Transients from the MCP detector are recorded with a 400 Msample/s 100 MHz digitizer (Acqiris DP310). The experiment is run at twice the repetition rate of FELICE allowing for the registration of reference mass spectra to correct for long-term source fluctuations.

The IR-MPD spectra for $[M, C, 2H]^+$ are measured by monitoring the fragmentation yield defined by $y = -\ln(P/(P + F))$ where P is the number of parent ions and F the number of fragment ions. The fragmentation yield is further normalized on the macropulse energy, as inferred from a fraction of the light

coupled out of the cavity. For the experiments described here, typical macropulse energies are in the range of 0.5−2 J.

For the Ta, W, and Pt systems, resonant excitation results in loss of atomic H. At the maxima of the vibrational resonances, a second H-loss can also be observed. Possible decompositions that would form M^+ cannot be observed because not all metal ions interact with methane and significant amounts of the bare cation are present in the molecular beam exiting the source. The loss channel of tungsten is consistent with previous results by Simon et al.[18] and is the lowest energy dissociation pathway according to the thermochemistry from Armentrout et al.[14] For tantalum, the known thermochemistry[16] identifies H atom loss as the lowest energy decomposition pathway for $[Ta,C,2H]^+$, although no TaC^+ product was observed in that study, presumably because it is indeed a high energy channel. For $[Pt,C,2H]^+$, the loss channel observed in previously reported experiments was loss of $[C,2H]$;[13,41] however, the known thermochemistry indicates that H loss is the lowest energy decomposition channel.[13] For Ir, resonant excitation yields formation of IrC^+, which is the lowest energy decomposition channel according to the thermochemistry of Li et al.[15]

Care has to be taken in the choice of fragment ion as the isotopic pattern of the metals may obscure the observation of fragment ions. Moreover, in the experiment not only $[M,C,2H]^+$ is produced, but also $[M,C,4H]^+$. It is assumed that the pressure in the reaction channel allows for the stabilization of these complexes through collisions with the helium carrier gas. Thus, we also ensured that products originating from $[M,C,4H]^+$ are not interfering with the $[M,C,2H]^+$ decomposition products, by monitoring the fragmentation into the channels of $[Ta,C,H]^+$, $[^{194}Pt,C,H]^+$, $[^{182}W,C,H]^+$, and $^{191}IrC^+$, respectively. At the strongest resonances, depletions of up to 15% of the parent ions are observed, which are mirrored in the appearance of signal in the fragment ion channels.

To vary the macropulse fluence in the experiment, the whole experimental apparatus can be translated along the FELICE laser beam. With a maximum translation of 300 mm from the focus and the 55 mm Rayleigh range of the FELICE optical beam, the fluence (at a fixed wavenumber) can be varied by a factor of 30. Variation of the fluence leads to a close to linear dependence of the fragmentation yield, as observed in previous experiments.[42,43] As the strongest resonances can become saturated and broadened at IR fluences where smaller features are barely visible, spectra were recorded at various but fixed distances from the focus. The focal distances at which spectra presented here were recorded are a compromise between visibility of small resonances and suppression of broadening effects. Typical fluences used range from 20 J/cm^2 at 300 cm^{-1} to 200 J/cm^2 at the highest frequencies probed.

DFT Calculations. To allow for structural assignment based on the IR-MPD spectra, density functional theory (DFT) calculations have been carried out. The present calculations are an extension of the results described previously for Pt[13] (with starting structures from Heinemann et al.[44]), W,[14] Ir,[15] and Ta,[16] and are primarily aimed at the interpretation of the observed IR-MPD spectra. Geometries reported in the previous publications for carbene and carbyne structures as well as for transition states between them have been reoptimized for the lowest spin states. For the $[Ir,C,2H]^+$ system, the experimental results led us to study a previously not considered carbyne structure. The B3LYP hybrid density functional[45,46] used in the previous publications is employed again, but now with a different basis set reflecting the progress in basis set development on the TM elements in particular. The def2-TZVPPD basis set[47] is used, which is a balanced triple-ζ basis set with two polarization and diffuse functions on all elements with an all-electron basis set for C and H and a small-core effective core potential def2-ECP for the heavier elements,[48] so that their 5s, 5p, 6s, 6p, and 5d electrons are explicitly treated in the basis set.

To compare the experimental spectra with calculated spectra, harmonic frequencies have been calculated and scaled by a global scaling factor of 0.939 to compensate for anharmonicity and experimental redshifting caused by the multiple photon nature of IR-MPD.[24] The global scaling factor is determined by a fitting procedure of the calculated spectrum of the lowest energy $[Pt,C,2H]^+$ structure to the experimental spectrum. All DFT calculations have been performed using the Gaussian 03 suite of programs.[49]

To compare the calculated spectra with the experimental IR-MPD spectra, the frequencies are convoluted with a Gaussian line shape function with an associated Gaussian width of 25 cm^{-1} (fwhm $\approx$ 60 cm^{-1}).

RESULTS AND DISCUSSION

DFT Calculations. The DFT calculations yield various stable structures for each system under study. The number and type of structures found varies. In general, each spin state considered has two minima: one of carbene and one of carbyne type. Depending on the element and spin state, these minima may or may not be affected by agostic interactions. For two spin states of W, three minima are found, as a competition between a C_{2v} and an agostically distorted carbene structure occurs. For each metal, only a single structure for $[M,C,2H]^+ + H_2$ with a relative energy below that of $M^+ + CH_4$ is found, except for the Ir complex, for which two such structures are located. For convenience, we refer to such species as being exothermically formed product ions.

The results from the DFT calculations are gathered in Table 1. The potential energy surfaces (PESs) and geometries of the systems are also graphically represented in the figures accompanying each section describing the experimental results for each system. In Table 1, the energies of the different species for the products ($[M,C,2H]^+ + H_2$) relative to the ground state of the reactants $M^+ + CH_4$ (M = Ta, W, Ir, Pt) are given taking into account the energy of the H_2 lost in formation. This choice of reference gives an immediate indication of whether the associated dehydrogenation reaction is exothermic or endothermic. Bond lengths and angles for the various carbene, carbyne, and transition state structures, respectively, can be found in the Supporting Information.

Platinum. In Figure 1, two spin multiplicity PESs for $[Pt,C,2H]^+$ products are shown with transition states between them. As the present calculations are aimed at elucidating the product structure, the formation pathways are not shown, but can be found in ref 13.

For $[Pt,C,2H]^+$, only the doublet and quartet states are considered as the sextet state is not reasonably accessible because it requires excitation to a 6p orbital. The two different geometries are a classic carbene (C_{2v} symmetry) and a carbyne type structure. The doublet carbene state is the lowest energy structure by more than 1 eV and the only exothermically formed product. In the $PtCH_2^+$ species, platinum uses two of the six valence orbitals (s and d) to form a σ− and π−bond with CH_2. This leaves seven electrons occupying the four remaining nonbonding orbitals on platinum, such that there are no empty orbitals on the metal. Therefore, there is no possibility for the C−H bond to donate

dx.doi.org/10.1021/jp400305k | J. Phys. Chem. A 2013, 117, 4115−4126

Table 1. Calculated Electronic Energy E, Vibrational Zero-Point Energy ZPE, and Relative Energy E_r of Reactants, $[M,C,2H]^+$ Products, and Their Transition States[a]

	term symbol	E (E_h)	ZPE (E_h)	E_r (eV)
H_2	$^1\Sigma_g^+$	−1.180021	0.009452	
CH_4	$^1A_1$	−40.539155	0.041879	
Ta^+	^1D	−56.519166		(1.90)
	^3P	−56.575286		(0.37)
	^5F	−56.588936		0.00
Ta^+CH_2	$^1A'$	−95.922130	0.020007	0.37
	$^3A''$	−95.937011	0.019817	*-0.04*
	$^5B_2$	−95.906140	0.019933	0.80
HTa^+CH	$^1A'$	−95.914226	0.017596	0.52
	$^3A''$	−95.892732	0.017061	1.09
	$^5A'$	−95.852096	0.015529	2.15
TS1	$^1A_1$	−95.916410	0.019218	0.51
	$^3A_1$	−95.933218	0.019085	0.04
	$^5A'$	−95.848943	0.014887	2.22
TS2	$^1A'$	−95.902587	0.016458	0.80
	$^3A''$	−95.879287	0.015588	1.41
W^+	^2X	−66.610538		(1.35)
	^4F	−66.630043		(0.82)
	^6D	−66.660018		0.00
W^+CH_2	$^2B_2$[b]	−105.979156	0.020814	0.77
	$^2A''$[c]	−105.996646	0.020004	0.27
	$^4B_2$[b]	−105.993402	0.020681	0.38
	$^4A''$[c]	−106.011288	0.019893	*-0.13*
	$^6A_1$	−105.984371	0.020737	0.63
HW^+CH	$^2A'$	−106.003305	0.018230	0.04
	$^4A'$	−105.965501	0.017598	1.06

	term symbol	E (E_h)	ZPE (E_h)	E_r (eV)
HW^+CH	$^6A'$	−105.909131	0.016045	2.55
TS1	$^2A'$	−105.977607	0.018908	0.76
	$^4A_2$	−106.006609	0.019002	−0.02
TS2	$^2A'$	−105.982966	0.016987	0.56
	^6A	−105.897725	0.014330	2.81
Ir^+	^1G	−103.875388		(1.98)
	^3F	−103.943388		(0.12)
	^5F	−103.948053		0.00
$Ir^+ CH_2$	$^1A_1$	−143.294408	0.021223	0.04
	$^3A_2$	−143.317804	0.021707	*-0.58*
	$^5A'$	−143.252717	0.018632	1.11
$HIr^+ CH$	$^1A'$	−143.324517	0.019323	*-0.83*
	$^3A'$	−143.285165	0.016934	0.18
	^5A	−143.203246	0.016151	2.39
TS	$^1A'$	−143.285919	0.018198	0.19
	$^3A'$	−143.257246	0.015406	0.90
	$^5A'$	−143.195006	0.014895	2.58
Pt^+	^4F	−118.943496		(0.78)
	^2D	−118.972134		0.00
$Pt^+ CH_2$	$^2A_1$	−158.333600	0.021781	*-0.35*
	$^4A''$	−158.261259	0.019702	1.56
$HPt^+ CH$	$^2A'$	−158.291344	0.017554	0.68
	^4A	−158.221394	0.016175	2.55
TS	$^2A'$	−158.271287	0.015680	1.18
	^4A	−158.212873	0.015086	2.75

[a] E_r is given relative to the energies of ground state reactants ($M^+ + CH_4$) including the energy of H_2. Italics indicate products that can be formed exothermically. Values in parentheses are relative to the ground state atomic ion. [b] Carbene-like. [c] Agostic structure.

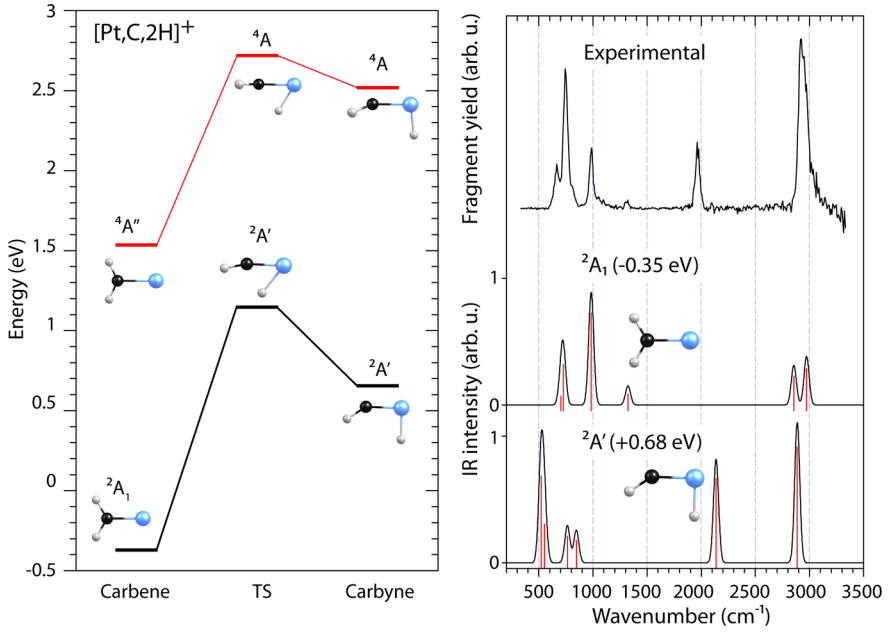

Figure 1. Schematic view (left) showing the $[Pt,C,2H]^+$ carbene and carbyne type minima and transition states between them for the doublet (black trace) and quartet (red trace) surfaces. Right: IR-MPD spectrum for $[Pt,C,2H]^+$ (top) and calculated spectra for the doublet carbene (middle trace) and carbyne structures (bottom). Energies from Table 1 are also indicated.

dx.doi.org/10.1021/jp400305k | J. Phys. Chem. A 2013, 117, 4115−4126

electron density to the metal and an agostic structure is not possible.

The right panel of Figure 1 shows the experimental IR-MPD spectrum of $[Pt,C,2H]^+$, compared with calculated spectra for two structures of doublet spin multiplicity, a C_{2v} carbene structure (middle), and a carbyne structure (bottom). The calculated spectra are depicted as stick spectra and convolutions. The calculated spectra for the quartet states are not shown, because these structures are almost 2 eV higher in energy. For the carbyne structures, the doublet and quartet spectra only differ in the IR intensity of the bands. The spectrum calculated for the quartet carbene structure is very different from that of the doublet carbene and compares unfavorably with the experimental spectrum.

The experimental IR-MPD spectrum exhibits distinct peaks centered at 743, 983, 1321, 1962, and 2925 cm^{-1}. The resonance on the low frequency side of the 743 cm^{-1} peak is interpreted as an additional band at 665 cm^{-1}. At first glance, one would be tempted to conclude that the experimental band at 1962 cm^{-1} appears most consistent with the carbyne structure (lower calculated spectrum) and thus that the six peaks are all $3N - 6$ fundamental vibrations for the system. However, a closer inspection of the calculated spectra reveals that the match between experimental and calculated spectrum for the carbyne structure is poor in the low-frequency range, below 1800 cm^{-1}, whereas the lowest energy C_{2v} carbene structure provides a very good agreement with the experiment in this region. The normal modes associated with the four low-frequency carbene vibrations are an in-plane bending motion at 702 cm^{-1}, a Pt−C stretching motion at 725 cm^{-1}, the out-of-plane bending motion of the hydrogens at 983 cm^{-1}, and a CH_2 scissoring motion at 1323 cm^{-1}. It is obvious that the experimentally observed resonance at 1962 cm^{-1} is not predicted for the carbene structure, but the frequency difference with the calculated mode at 2137 cm^{-1} for the carbyne structure, the Pt−H stretching vibration, is unsatisfactorily large.

Two C−H stretching modes, a symmetric and an antisymmetric combination, are predicted for the carbene at 2855 and 2973 cm^{-1}. In the experimental IR-MPD spectrum only a single resonance is observed. This resonance is rather broad, about 150 cm^{-1} fwhm, suggesting that the two predicted modes may be unresolved. This broadening can partly be explained by the rotational substructure of the observed bands. Because the hydrogen atoms in a C_{2v} structure are equivalent, the rotational K states (the projection of the rotational quantum number $\vec{J}$ on the principal rotational axis) are populated according to nuclear spin statistics. For a perpendicular band, the selection rules are $\Delta K = \pm 1$ and in a molecular beam one expects to observe three strong sub-Q-branches $(K' = 0 \leftarrow K'' = 1)$, $(K' = 1 \leftarrow K'' = 1)$ and $(K' = 2 \leftarrow K'' = 1)$, spaced by $2(A-B)$, or about 18 cm^{-1}. Such splitting has been previously observed for the C_{2v} Ca^+-H_2O ion.[50] If the cooling of the ions is not optimal, more populated K-states will contribute and broaden the rotational structure. The broadening effects characteristic for IR-MPD are then responsible for the further overlap of the two vibrational bands.

With the exception of the 1962 cm^{-1} resonance, the agreement with the calculated spectrum for the carbene is significantly better than for the carbyne. For this reason, the spectrum is assigned to the doublet spin multiplicity C_{2v} carbene structure. The question then remains what the nature of the 1962 cm^{-1} resonance is. The band may be assigned as the first overtone of the out-of-plane bend, but this would indicate a very small anharmonicity (0.2%), which belies the high intensity observed. Alternatively, this band could be a combination of the CH_2 scissor and in-plane bending vibrations. A calculation of anharmonic vibrational frequencies for $[Pt,C,2H]^+$ indicates that the line position for the overtone of the CH_2 out-of-plane bending vibration is close to the combination band between the CH_2 scissor and in-plane bending vibrations, and that the combination band indeed exhibits a larger anharmonicity than the overtone, which could enhance its intensity. Combination bands have been observed previously in IR multiple photon excitation spectra, for example, for the fullerene C_{60}.[51]

Although the band positions are accurately described by theory below 1500 cm^{-1}, the predicted intensities do not match the experimental spectrum particularly well. It must be stressed that the IR-MP excitation mechanism can induce discrepancies between intensities of resonances in IR-MPD spectra and (calculated) linear absorption spectra.[52] Such effects may also explain the slight mismatch in the frequency spacing between the calculated vibrational modes at 702 and 725 cm^{-1} and the modes observed at 665 and 743 cm^{-1}.

To check whether the comparison between experimental and calculated line positions can be improved, several additional calculations were carried out. To exclude problems with the ECP, an all-electron quasi-relativistic zero-order regular approximation (ZORA) calculation was done. Neither these, nor scalar-relativistic calculations or two-component calculations that include spin−orbit coupling led to appreciable differences in the calculated spectra. We thus conclude that the calculations of Figure 1 are at a sufficiently high level and that the IR-MPD mechanism is responsible for the discrepancies.

Tantalum. In Figure 2, three spin multiplicity PESs for the product of methane dehydrogenation by Ta^+ are shown. For $[Ta,C,2H]^+$, the PES is more complex than for $[Pt,C,2H]^+$. Besides minima for carbene and carbyne type geometries, there is a distorted carbene type structure resulting from an agostic interaction between a C−H bond and an empty Ta 5d orbital, the in-plane π-like orbital. In fact, the triplet spin state of this C_s structure is the only exothermically formed product. The lowest energy orbital occupancy is a $^3A''$ state, although Parke et al.[16] also located a $^3A'$ state only 0.032 eV higher in energy. These states differ only in which of the two δ-like orbitals is occupied. Because neither of these orbitals interacts strongly with the CH_2 ligand their spectra are essentially identical. The agostic minima give rise to a double-well potential (not shown) with a low-lying $^3A_1$ transition state (TS1) having C_{2v} symmetry associated with in-plane wagging of the CH_2 group. A similar TS1 ($^1A_1$) is found on the singlet surface.

The top right panel of Figure 2 shows the experimental IR-MPD spectrum of $[Ta,C,2H]^+$, compared with calculated spectra for the three lowest energy structures: two distorted carbene type structures, of triplet (second trace) and singlet spin multiplicity (third trace), and a singlet carbyne structure (bottom trace). The experimental IR-MPD spectrum exhibits four peaks centered at 687, 830, 1330, and 3027 cm^{-1}. The 1330 cm^{-1} resonance has a shoulder on the red side at 1179 cm^{-1}. The assignment of the experimental IR-MPD spectrum is rather straightforward: of the three lowest energy structures, the calculated spectrum for the triplet ground state distorted carbene structure provides an excellent match with the experimental spectrum.

In the calculated spectrum for this triplet carbene structure, the 668 cm^{-1} calculated mode is associated with an out-of-plane bending vibration of the hydrogens. The vibration at 808 cm^{-1}

dx.doi.org/10.1021/jp400305k | J. Phys. Chem. A 2013, 117, 4115−4126

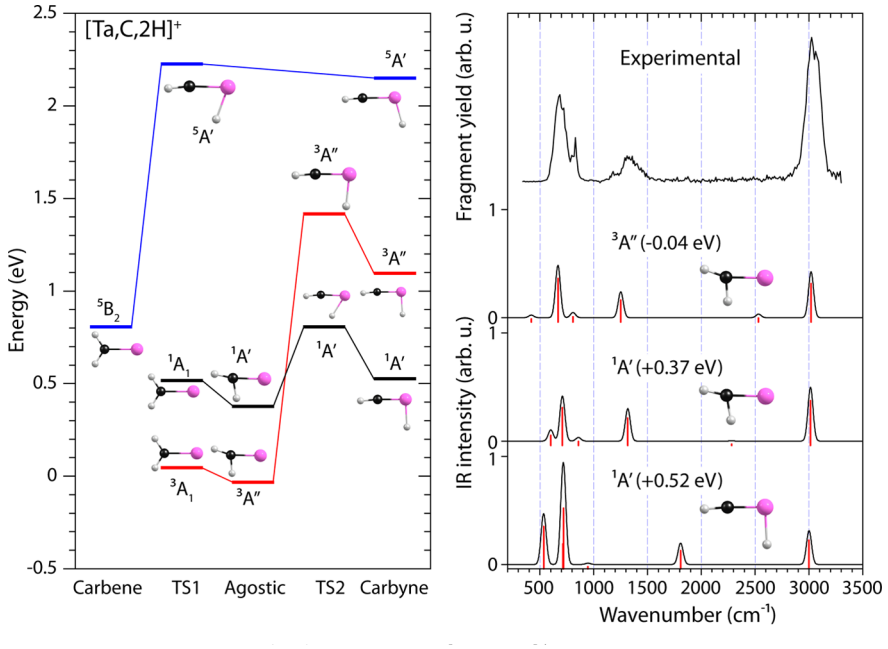

Figure 2. Schematic view (left) showing the $[Ta,C,2H]^+$ carbene, carbyne, and agostically distorted type minima and transition states between them for the singlet (black trace), triplet (red trace), and quintet (blue traces) surfaces. Right: IR-MPD spectrum for $[Ta,C,2H]^+$ (top) and calculated spectra for the distorted carbene, triplet (second trace) and singlet (third trace), and singlet carbyne structures (bottom trace). Energies from Table 1 are also indicated.

is due to the Ta−C stretching vibration, that at 1251 cm^{-1} is the CH_2 scissoring mode, and the mode at 3020 cm^{-1} is the stretching of the C−H that is not involved in the agostic interaction.

The calculated spectrum shows two modes, at 420 (in-plane bending of the CH_2 group) and 2532 cm^{-1}, for which the line positions have not been experimentally confirmed, even at the highest fluence available, probably as a result of their very low calculated absorption cross sections. The position of the mode at 2532 cm^{-1}, the C−H stretching vibration where the hydrogen is part of the agostic two-electron bond, is very diagnostic for the strength of the agostic interaction. For the singlet spin state of the distorted carbene structure, this mode shifts ≈250 cm^{-1} to the red, indicating a stronger agostic interaction. This is reflected in the smaller Ta−C−H angle of 78.6° for the singlet (85.1° for the triplet) implying a larger overlap of the hydrogen s-orbital with the tantalum d-orbital. The second unobserved triplet band at 420 cm^{-1} shifts to the blue for the singlet structure, positioning it close to the strong band at 687 cm^{-1}. Because of the good correlation between the experimental spectrum and the calculated frequencies of the triplet agostically distorted carbene structure, the global minimum, the experimental spectrum is assigned to this structure, in agreement with the conclusions of Parke et al.[16]

What remains unexplained is the somewhat weaker feature at 1179 cm^{-1}. One possible explanation is that this feature corresponds to the predicted band at 1251 cm^{-1}, such that the 1330 cm^{-1} band is then assigned as an overtone of the 687 cm^{-1} band (3.3% anharmonicity). Alternatively, this could be evidence for the $^1A'$ state (calculated band at 1316 cm^{-1}). As the singlet carbene structure has vibrational frequencies that are only slightly shifted from those of the triplet carbene, its presence cannot be fully excluded.

Tungsten. In Figure 3, three spin multiplicity PESs (doublet, quartet, and sextet) for $[W,C,2H]^+$ are shown. Empty W^+ d-orbitals allow for agostic interactions and the PES correspondingly exhibits minima for C_{2v} carbene structures, for distorted carbene structures, and for carbyne structures. In comparison to $[Ta,C,2H]^+$, two more minima on the $[W,C,2H]^+$ PES are found. For the doublet and quartet spin states, there is a competition between agostic distortion and a C_{2v} structure for the carbene, and both types are found to be stable. On the sextet PES, only a stable C_{2v} structure is found. For all spin states, a stable carbyne structure is found. The lowest energy structure is the $^4A''$ state of the distorted carbene, the only species that can be formed exothermically from reaction of W^+ with methane. This species has a $^4A_2$ transition state associated with in-plane wagging of the CH_2 group only 0.113 eV higher in energy. Also, a stable $^4B_2$ state having C_{2v} symmetry exists.[14] Distortions of this state and the quartet carbyne species were explored thoroughly, but no transition states connecting either structure with other quartet species could be located.

In their study of the geometric structure of the $[M,C,2H]^+$ (M = La, Hf, Ta, W, Re, Os, Ir, Pt, Au) species, Irikura and Goddard[17] only investigated the C_{2v} symmetric structures in detail. Later, Simon et al.[18] performed a more rigorous investigation of the possible structures of the $[W,C,2H]^+$ species, considering the carbene, agostic, and carbyne types of geometries. They used several basis sets at the B3LYP, CCSD(T), and CASPT2 levels of theory and even included spin−orbit (SO) coupling. They found the same ordering of energies before including SO coupling as in the current study. However, including SO coupling resulted in the carbyne structure having lower energy than the agostic carbene structure. Armentrout et al.[14] also investigated these geometries and their results before including SO coupling essentially reproduce the results found by Simon et al.[18] Upon inclusion of an approximate correction for the SO coupling, the agostic structure is still lower in energy than the carbyne structure.[14] Both publications report only

dx.doi.org/10.1021/jp400305k | J. Phys. Chem. A 2013, 117, 4115−4126

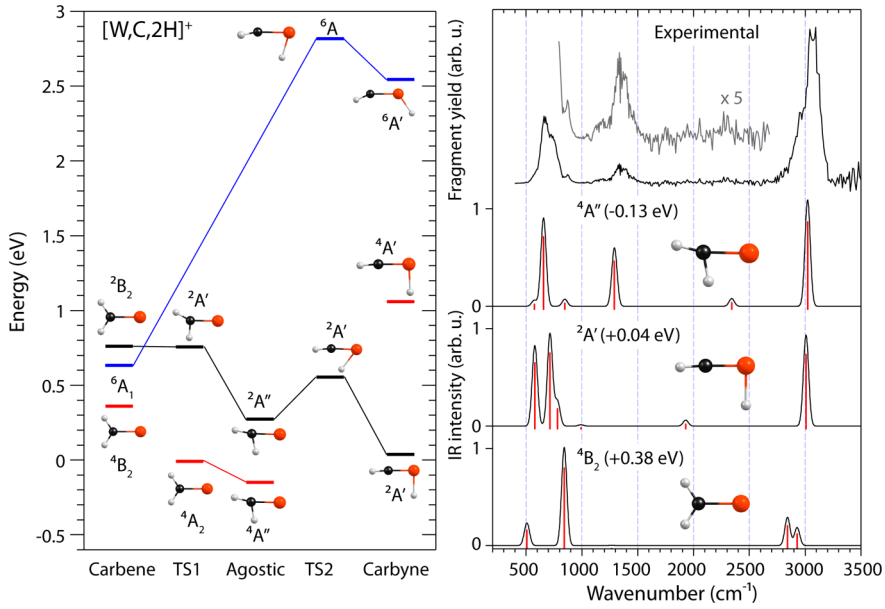

Figure 3. Schematic view (left) showing the $[W,C,2H]^+$ carbene, carbyne, and agostically distorted type minima, and transition states between them for the doublet (black trace), quartet (red trace), and sextet (blue traces) surfaces. Right: IR-MPD spectrum for $[W,C,2H]^+$ (top) and calculated spectra for the quartet distorted carbene (second trace), doublet carbyne (third trace), and quartet C_{2v} carbene structures (bottom trace). Energies from Table 1 are also indicated.

small differences in energy (less than 0.1 eV) between these species.

The top right panel of Figure 3 shows the experimental IR-MPD spectrum of $[W,C,2H]^+$. The experimental spectrum shows only three main resonances centered at 661, 1336, and 3070 cm^{-1}. The 661 cm^{-1} peak has a satellite peak at 878 cm^{-1}, and the asymmetric line shape of the 3070 cm^{-1} resonance suggests two bands. A fit to two Gaussian lineshapes yields resonances at 2937 and 3073 cm^{-1}.

Below the experimental spectrum are calculated spectra for the three lowest energy structures: a distorted quartet carbene (second trace), a doublet carbyne structure (third trace), and a quartet C_{2v} carbene (bottom trace). The geometric structure largely determines the calculated harmonic frequencies as only minor frequency shifts are found for the different spin states. Therefore only the calculated spectra belonging to the lowest energy spin state is shown for each geometry.

The quartet agostic structure, which is the global minimum and the only structure exothermically accessible from the $W^+ + CH_4$ reactants, shows the best match with the experimental spectrum. Its calculated spectrum shows an intense peak at 656 cm^{-1} from the out-of-plane bending mode with a weak one nearby at 847 cm^{-1} due to stretching of the W−C bond. A moderately intense peak is located at 1292 cm^{-1} (CH_2 scissoring mode) and an intense peak at 3022 cm^{-1} (stretching mode of the C−H furthest away from the W). The lowest frequency calculated vibration, the in-plane bending mode at 573 cm^{-1}, is visible in the experimental spectrum as a shoulder on the lowest energy peak. The stretching of the C−H bond perpendicular to the W−C bond at 2342 cm^{-1} has very low intensity, which probably explains why it is not readily visible in the experimental spectrum. However, the 5×-zoom shown in Figure 3 shows a slight increase in signal centered around 2300 cm^{-1} that may be interpreted as a weak resonance.

While the carbene structure is energetically favored in the calculations and its presence is evidenced by the 1336 cm^{-1} resonance, we cannot rule out the presence of the carbyne as its resonances are screened by those of the carbene structure. The only diagnostic mode for the carbyne, the W−H stretching vibration at 1930 cm^{-1}, is too weak to be detected. The asymmetric lineshape of the 3070 cm^{-1} resonance may point to the presence of the carbyne.

These results confirm the calculations presented by Simon et al.[18] predicting the importance of an agostic distortion. The presence of the carbyne structure, energetically favored by these authors' calculations, can neither be confirmed nor ruled out.

Iridium. Figure 4 shows the PESs of three spin states of the $[Ir,C,2H]^+$ product. The first investigation of the geometric structure was reported by Irikura and Goddard,[17] who discarded the carbyne structure as a serious possibility for all third-row metals, including iridium. In the same year, Perry et al.[53] published a theoretical investigation into why Ir is the most efficient transition-metal ion for dehydrogenation of methane in the gas phase. They correctly remark that Ir is one of the few metals capable of forming four covalent bonds, but recognize its importance only for the intermediate structures and not for the $[Ir,C,2H]^+$ species. They found a $^3A_2$ ground state carbene structure that was only slightly exothermic (0.13 eV) relative to the reactants, leading to the conclusion that the Ir^+ methane dehydrogenation efficiency is kinetic. Li et al.[15] report a $^3A_2$ structure with a substantially lower energy at 0.55 eV below that of the reactants. We find the same structure with a similar exothermicity of 0.58 eV, Table 1.

In contrast to the other metals discussed here, we find a second exothermically formed product: a carbyne structure on the singlet surface, which has not previously been considered, is found with a relative stability of −0.83 eV. Along with the experimental spectrum of $[Ir,C,2H]^+$ in Figure 4, the calculated spectra are shown for the singlet carbyne and triplet carbene structures, as well as for an endothermically formed triplet carbyne structure. Although lower in energy than the triplet carbyne (+0.18 eV), the spectrum for the singlet carbene (+0.04 eV) is not displayed as it is very similar to that for the triplet carbene.

dx.doi.org/10.1021/jp400305k | J. Phys. Chem. A 2013, 117, 4115−4126

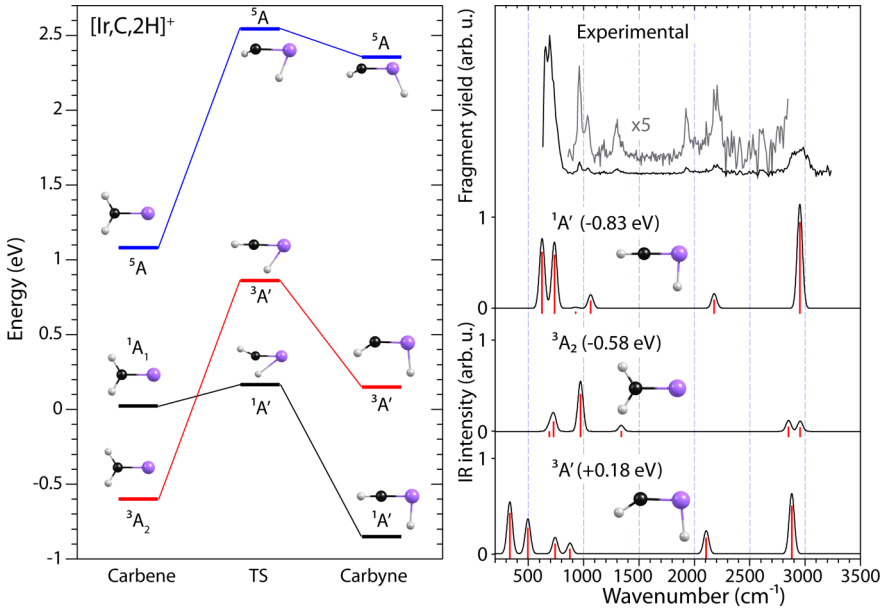

Figure 4. Schematic view (left) showing the $[Ir,C,2H]^+$ carbene and carbyne type minima and transition states between them for the singlet (black trace), triplet (red trace), and quintet (blue traces) surfaces. Right: IR-MPD spectrum for $[Ir,C,2H]^+$ (top) and calculated spectra for the singlet carbyne (second trace), triplet carbene (third trace), and triplet carbyne structures (bottom trace). Energies from Table 1 are also indicated.

Intriguingly, the carbyne H−Ir−C angle for the singlet carbyne is clearly distorted from the formal 90°, expected for bonding to sd hybridized orbitals on the metal, to 86.8°, whereas the same angle in its triplet carbyne structure is 97.2°. This indication of an interaction between the carbon and the hydrogen is enforced by the blueshift in the calculated Ir−H stretching vibration from 2107 cm^{-1} (triplet) to 2179 cm^{-1} (singlet).

Note that an agostic interaction cannot occur for $IrCH_2^+$ on the triplet surface. Here, iridium uses two of the six valence orbitals (6s and 5d) to form a σ- and π-bond with CH_2. This leaves six electrons occupying the four remaining nonbonding orbitals on iridium, such that there are no empty orbitals on the metal for a triplet state, but there can be for a singlet. As shown in Figure 4, the four covalent bonds in the carbyne structure make it energetically favorable enough for the system to cross from the triplet surface to the singlet surface, implying a rearrangement of the Ir d-electrons. Although a stable $^1A_1$ carbene structure is located, the empty 5d orbital on this species allows the TS associated with the agostic interaction to be low in energy. Interestingly, unlike the early TMs, the agostic interaction in this case does not stop at a distortion but continues to form the IrH bond and cleave the CH bond.

The experimental spectrum of the $[Ir,C,2H]^+$ species shows a strong resonance just below 700 cm^{-1} and a broad one centered around 2940 cm^{-1}. A closer inspection reveals that the low-frequency band consists of two separate peaks at 656 and 694 cm^{-1}. A 5×-zoom of the spectrum between the two intense bands is also shown in Figure 4, displaying five additional resonances at 961, 1034, 1301, 1933, and 2198 cm^{-1}. This total number of eight bands is too large to be explained by the fundamental transitions of a single structure.

Comparison of experimental and calculated spectra in Figure 4 appears to rule out the carbene structure as the major contributor to the observed spectrum. The carbene structure has no resonances around 2000 cm^{-1}, and its strongest resonance is predicted at 956 cm^{-1}, where only weaker resonances are found. The calculated spectrum of the singlet carbyne structure with its double peak structure around 680 cm^{-1} compares more favorably with the experimental spectrum. Each of the predicted fundamental transitions for this structure corresponds to a resonance observed in the experimental spectrum, including the diagnostic Ir−H stretching vibration calculated at 2179 cm^{-1}. The relative intensity of the observed resonance at 2940 cm^{-1} is lower than what would be expected from the calculated spectra.

Fundamental transitions for the singlet carbyne structure cannot explain the resonances at 961, 1301, and 1933 cm^{-1}. We first consider the line positions of the triplet carbene structure: two resonances around 710 cm^{-1}, one at 956 and 1338 cm^{-1}, and two around 2900 cm^{-1}. The four resonances around 710 and 2900 cm^{-1} coincide with strong resonances of the carbyne and are obscured from observation. The two remaining fundamentals at 956 and 1338 cm^{-1}, respectively, coincide with observed resonances at 961 and 1301 cm^{-1}. As the carbene structure can be formed exothermically from Ir^+ and methane, it is conceivable that this structure is also formed in competition with the singlet carbyne structure.

This leaves the band at 1933 cm^{-1} unaccounted for. We note that the calculated spectrum for the doublet C_{2v} carbene structure of Pt^+CH_2 is very similar to the spectrum calculated for the Ir^+CH_2 carbene structure considered here. The $[Pt,C,2H]^+$ spectrum (Figure 1) exhibits an unexplained resonance at 1962 cm^{-1}, close to the band observed here at 1933 cm^{-1}. For $[Pt,C,2H]^+$, where no plausible alternative candidate structures are available, this band is tentatively assigned as a combination band. For $[Ir,C,2H]^+$, a similar assignment is suggested and the band at 1933 cm^{-1} is attributed to a combination band of the CH_2 scissor and in-plane bending vibrations of the carbene structure.

Previously, only the carbene structure for $[Ir,C,2H]^+$ had been considered. Nonetheless, the carbyne structure is found here as the lowest energy $[Ir,C,2H]^+$ structure, and the experimental spectrum suggests that this species is the dominant product formed by methane dehydrogenation.

Formation of $HIrCH^+$. The PES for interaction of Ir^+ with methane has been extensively studied theoretically,[53,54] most recently by Li et al.[15] None of these studies considered the formation of an $HIrCH^+$ species. We therefore explore the

dx.doi.org/10.1021/jp400305k | J. Phys. Chem. A 2013, 117, 4115−4126

Table 2. Calculated Electronic Energy E, Vibrational Zero-Point Energy ZPE[a], and Relative Energy E_r of Species along the $[Ir,C,4H]^+$ Potential Energy Surface[b]

species	term symbol	E (E_h)	ZPE (E_h)	E_r (eV) this work	E_r (eV) ref 15
$Ir^+(CH_4)$	$^1A'$	−144.526824	0.042665	−1.13	0.18
	$^3A''$	−144.536343	0.042791	−1.39	−1.27
	$^5A''$	−144.504238	0.043852	−0.48	−0.53
TS1	$^1A'$	−144.526647	0.040986 (469)	−1.17	0.13
	$^3A''$	−144.518272	0.040791 (826)	−0.95	−1.30
	$^5A''$	−144.439419	0.036392 (408)	1.08	0.95
$HIrCH_3^+$	$^1A'$	−144.547397	0.041432	−1.72	−0.88
	$^3A''$	−144.557579	0.041532	−2.00	−1.95
	$^5A''$	−144.482142	0.038830	−0.02	−0.03
TS3	^1A	−144.535908	0.038930 (739)	−1.48	−0.89
	^3A	−144.507145	0.035118 (732)	−0.80	−0.74
$H_2IrCH_2^+$	$^1A'$	−144.579836	0.039929	−2.65	−2.57
	$^3A''$	−144.517028	0.036309	−1.04	−1.00
TS4	^3A	−144.510838	0.035087 (479)	−0.90	−0.84
$IrCH_2^+(H_2)$	$^1A'$	collapses to $H_2IrCH_2^+$			
	$^3A_2$	−144.522568	0.038785	−1.12	−1.08
TS5 (from $H_2IrCH_2^+$)	^1A	−144.509469	0.034150 (732)	−0.89	
	^3A	−144.465770	0.032579 (1031)	0.25	
H_3IrCH^+	^1A	−144.515355	0.035252	−1.02	
	$^3A''$	−144.486876	0.033794	−0.28	
TS6	^1A	−144.510903	0.033287 (525)	−0.95	
	^3A	−144.485292	0.032317 (682)	−0.28	
$(H_2)HIrCH^+$	$^1A'$	−144.532236	0.036428	−1.45	
	^3A	−144.488169	0.033985	−0.32	

[a]Imaginary frequencies in cm^{-1} shown in parentheses. [b]E_r is given relative to the energies of ground state reactants ($Ir^+ + CH_4$).

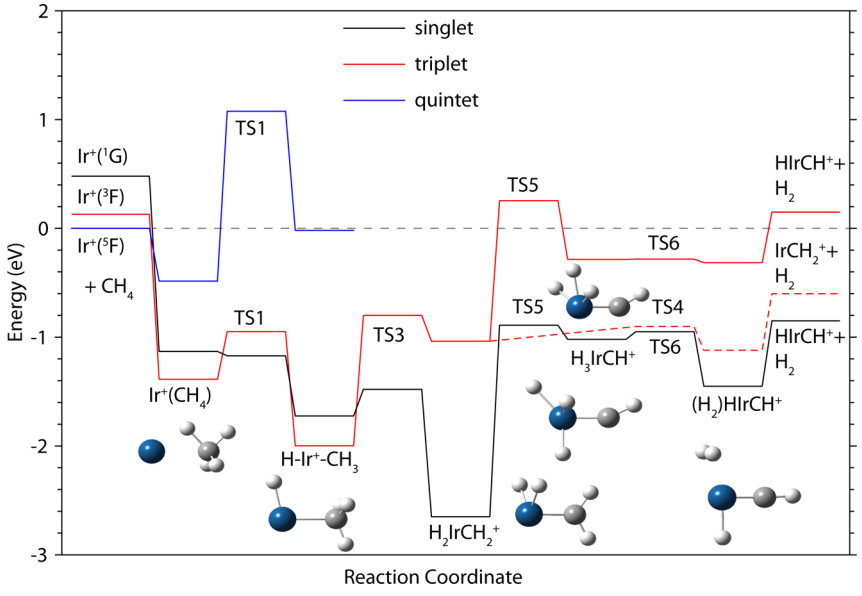

Figure 5. $[Ir,C,4H]^+$ potential energy surface derived from theoretical results. The relative energies of all species are based on ab initio calculations, and can be found in Table 2. Singlet (black trace), triplet (red trace), and quintet (blue traces) surfaces are indicated along with the lowest energy structures of all intermediates. Both the singlet and triplet structures of H_3IrCH^+ are shown.

formation of this species from $Ir^+ + CH_4$ reactants using the same level of theory as discussed above. The results are presented in Table 2 and Figure 5, with nomenclature consistent with the previous work. For intermediates and transition states (TS) identified previously, the present results largely reproduce the relative energies calculated at the B3LYP/HW+/6-311++G(3df,3p) level of theory (average difference of 0.1 ± 0.1 eV for 11 species). The main exception is that lower energy states for $Ir^+(CH_4)$, ^{1}TS1, $HIrCH_3^+$, and ^{1}TS3 (by 0.6–1.3 eV) are found along the singlet surface in the present work, which is likely a result of spin contamination in the present work, with $S(S+1)$ values of 0.99, 0.99, 0.98, and 0.69, respectively, rather than 0.0 for true singlet species. At the present level of theory, these intermediates collapse to $H_2IrCH_2^+$ along singlet surfaces that

dx.doi.org/10.1021/jp400305k | J. Phys. Chem. A 2013, 117, 4115−4126

are not spin contaminated, a result that is consistent with the previous work[15] where only pure singlet species were included. Thus these discrepancies do not change the qualitative character of the surfaces shown.

A detailed discussion of the pathway from the ground state (GS) $Ir^+(^5F)$ + CH_4 ($^1A_{1g}$) reactants to the $H_2IrCH_2^+$ dihydride iridium carbene cation intermediate can be found in previous work.[15] The key features are that a crossing from the quintet surface to the triplet surface must occur in the entrance channel. On the uncontaminated singlet surface of Li et al.,[15] $Ir^+(^1D/G)$ + CH_4 spontaneously forms $H_2IrCH_2^+$ with no intervening stable intermediates. Further, the coupling between the triplet and singlet surface occurs in the vicinity of TS3, between the $HIrCH_3^+$ and $H_2IrCH_2^+$ intermediates. On the present surfaces of Figure 5, this coupling can occur anywhere from the entrance channel to TS3. Note that singlet $H_2IrCH_2^+$ ($^1A'$) is the global minimum on the potential energy surface, as found in all previous work. Also in previous work, it was found that the dihydride intermediate can proceed along the singlet surface to directly eliminate dihydrogen and form the $IrCH_2^+$ ($^1A_1$) carbene, a product that lies 0.04 eV above the GS reactants, Table 1. The reverse process, activation of H_2 by $IrCH_2^+$ ($^1A_1$) to form $H_2IrCH_2^+$ ($^1A'$) is spontaneous with no stable intermediates on the reaction path.[15]

To form $HIrCH^+$ ($^1A'$) + H_2 from $H_2IrCH_2^+$, the system passes over ^{1}TS5 in which another hydrogen migrates from carbon to iridium forming the trihydride carbyne, H_3IrCH^+, which lies 1.02 eV below the GS reactants. This species is relatively high in energy because Ir^+ can readily form only four covalent bonds using its s and d valence orbitals. Indeed, the IrC bond length of 1.703 Å lies between that of the double bond in $IrCH_2^+$ (1.797 Å) and the triple bond in $HIrCH^+$ (1.654 Å), and one of the IrH bond lengths is quite extended, 1.654 Å, compared to the other two, 1.550 and 1.590 Å, or that in $HIrCH^+$, 1.557 Å. From H_3IrCH^+, two hydrogen atoms can combine across ^{1}TS6 to form $(H_2)HIrCH^+$ ($^1A'$), lying 1.45 eV below the GS reactants. H_2 loss from this intermediate requires only 0.60 eV. The product asymptote is the highest energy species along this dissociation pathway, however, both ^{1}TS5 and ^{1}TS6 are within 0.10 eV. This is the lowest energy dissociation pathway along any spin surface, with the formation of $IrCH_2^+$ ($^3A_2$) + H_2 lying 0.25 eV higher in energy (also shown in Figure 5, dashed line). Thus, reaction of Ir^+ with methane can lead to formation of both $HIrCH^+$ ($^1A'$) and $IrCH_2^+$ ($^3A_2$) with no barriers in excess of the product asymptotes and the former channel being thermodynamically favored. This is consistent with the spectroscopic observations made here.

We also examined formation of $HIrCH^+$ ($^3A'$) + H_2, which is endothermic by 0.18 eV from GS reactants. Furthermore, formation of this species requires passing over ^{3}TS5, which lies even higher in energy, 0.25 eV above the reactants. Here, H_3IrCH^+ ($^3A''$) lies only 3 meV below ^{3}TS6 and is 40 meV less stable than $(H_2)HIrCH^+$ (^3A). Loss of H_2 from this complex requires only 0.47 eV. Overall, formation of this species should not be competitive in the reaction of ground state Ir^+ + CH_4.

DISCUSSION

The aim of the study conducted here has been to investigate by IR spectroscopy the structures of the $[M,C,2H]^+$ products from methane dehydrogenation by the four 5d TM cations: tantalum, tungsten, iridium, and platinum. Two types of structures can be distinguished, a carbene-type and a hydrido-methylidyne (carbyne) structure. If suitable empty orbitals are present at the metal, an agostic interaction with a C−H bond can occur. Given the need for an empty 5d orbital, one naively might expect that agostic interactions would be present for the two early TMs only, and that Ir and Pt would not be affected. In fact, every element studied except Ir^+ fulfills those expectations. The structure found for $[Pt,C,2H]^+$ is readily assigned as a classical C_{2v} structure, as was predicted previously.[17] Ta^+ and W^+ form carbene structures that are strongly distorted by agostic interactions, which is again in line with previous reports.[16,18] Although the present study unambiguously proves that the structure of $[W,C,2H]^+$ is a distorted carbene structure, the theoretical findings of Simon et al.[18] have clearly demonstrated that hydrido-carbyne structures can be competitive in energy. It is therefore very interesting that the $[Ir,C,2H]^+$ structure is now established as a hydrido-carbyne, which can only occur for the low-spin singlet state.

From the current findings, it can be expected that $[M,C,2H]^+$ structures for Re^+ and Os^+ will be carbenes on high-spin surfaces (quintet and quartet/sextet, respectively), as found in previous calculations.[55,56] In analogy to the Ir case, an electronic rearrangement may occur to cross to lower spin surfaces. In the competition between carbene and carbyne structures, the former will then be susceptible to agostic interactions.

Spectroscopically, the difference between carbene and hydrido-carbyne structures should be rather straightforward to detect by the presence of a resonance at frequencies characteristic for the M-H stretching vibration.[57] A symmetric carbene structure gives rise to two peaks close together around 3000 cm^{-1} belonging to symmetric and antisymmetric C−H stretches of the CH_2 group. While the current technique is clearly structure sensitive, two resonances were not observed for the carbene structure of $[Pt,C,2H]^+$. Broadening effects can account for not resolving two bands in one experimentally recorded resonance. An agostic structure should reveal itself because the H directly interacting with the metal cannot vibrate as freely as the unbound H. For a distorted carbene structure, this results in a redshift of the vibrational frequency for the C−H stretching vibration. Unfortunately, this band is predicted to be weak such that for the distorted agostic carbene of $[Ta,C,2H]^+$ this band could not be observed; however, such a band is observed for $[W,C,2H]^+$. For the metal hydride of the carbyne structure, an M-H stretch is expected between 1500 and 2200 cm^{-1}, although it is often weak.[57] Here, such a weak band is observed for the $HIrCH^+$ species.

Finally, the mere fact that these $[M,C,2H]^+$ structures can be elucidated through IR-MPD spectroscopy is a remarkable finding. While IR-MPD was observed for neutral NH_3 upon excitation by a line-tunable CO_2 laser previously, the recording of the present spectra may be considered a landmark, since, to the best of our knowledge, no IR-MPD spectra for four-atomic ions have been recorded over such a large IR spectral range.

In the spectral range addressed in this work, it has been possible to observe resonances with calculated IR intensities as low as 8 km/mol. Although it is difficult to extrapolate this value to other systems because of different IVR rates and binding energies, this lower limit is substantially higher than that for several PAH cations recently studied with FELICE where bands of 1 km/mol could be observed.[58] The difference is attributed to the fact that the PAH cations were studied in an effusive beam which travels substantially slower than the current supersonic beam. This results in an irradiation of the PAH cations over the full duration of the FELICE macropulse, whereas the interaction between $[M,C,2H]^+$ species and the

dx.doi.org/10.1021/jp400305k | J. Phys. Chem. A 2013, 117, 4115−4126

FELICE laser pulse is limited to the transit time of the molecular beam through the FELICE beam.

As in most experiments using IR-MPD, the vibrational bands are broadened and red-shifted. In the current work, the broadening and redshifting are unusually large, which may be attributed to the sequential absorption of multiple photons in one coordinate before IVR is able to diffuse the energy in these small molecules. However, to investigate such effects is experimentally very difficult.

CONCLUSION

The IR-MPD spectra of the $[M,C,2H]^+$ (M = Ta, W, Ir, Pt) methane dehydrogenation products have been measured over the 300−3500 cm^{-1} spectral range. These are among the smallest molecular systems studied using IR-MPD spectroscopy. The multiple-photon nature of the technique and the difficulty in exciting smaller systems are reflected in a relatively large redshift of the vibrational frequencies with respect to the calculated linear absorption spectra, requiring a relatively small scaling factor of 0.939 for the calculated harmonic frequencies.

For three of the four systems, the experimental spectrum is uniquely assigned to the lowest energy structure, which is formed exothermically from M^+ + methane in all cases. For Ta^+, W^+, and Pt^+, this is a carbene structure. Agostic interactions distort the carbene structures for Ta^+ and W^+ from the classical C_{2v} symmetry structure. For Ir^+, the spectrum is assigned to a hydrido-carbyne structure, but a C_{2v} carbene structure slightly higher in energy, yet still exothermically formed, could account for some of the minor spectral features observed that cannot be attributed to the hydrido-carbyne structure. Two structures can be formed exothermically because of the ability of the $[Ir,C,2H]^+$ system to cross from the triplet to the singlet surface. The ability to cross to lower-spin surfaces should make the $[Os,C,2H]^+$ product, not studied here, susceptible for agostic distortions as well, and this is likewise a possibility in the $[Re,C,2H]^+$ system characterized by other means previously.[55]

ASSOCIATED CONTENT

Supporting Information

Bond lengths and angles for the various carbene, carbyne, and transition state structures, respectively. This material is available free of charge via the Internet at http://pubs.acs.org.

AUTHOR INFORMATION

Corresponding Author

*E-mail: j.bakker@science.ru.nl (J.M.B.), armentrout@chem.utah.edu (P.B.A.).

Notes

The authors declare no competing financial interest.

ACKNOWLEDGMENTS

This work is part of the research program of the "Stichting voor Fundamenteel Onderzoek der Materie (FOM)", and receives support from the National Science Foundation through Grants CHE-1049580 and PIRE-0730072. The construction of the FELICE beamline was funded by the "Nederlandse Organisatie voor Wetenschappelijk Onderzoek" (NWO) through the NWO-Groot scheme. We thank the FELIX staff for their assistance and Dr. A. Fielicke for the use of the iridium sample. We gratefully acknowledge Prof. C. van Wüllen for performing the ZORA, scalar-relativistic, and two-component calculations. We thank the referee for helpful suggestions on the interpretation of the $[Pt,C,2H]^+$ spectrum.

REFERENCES

(1) Bharadwaj, S. S.; Schmidt, L. D. Catalytic Partial Oxidation of Natural-Gas to Syngas. *Fuel Process. Technol.* **1995**, *42*, 109−127.

(2) Lee, Y. J.; Hong, S. I.; Moon, D. J. Studies on the Steam and CO_2 Reforming of Methane for GTL-FPSO Applications. *Catal. Today* **2011**, *174*, 31−36.

(3) Labinger, J. A.; Bercaw, J. E. Understanding and Exploiting C-H Bond Activation. *Nature* **2002**, *417*, 507−514.

(4) Irikura, K. K.; Beauchamp, J. L. Osmium Tetroxide and its Fragment Ions in the Gas Phase: Reactivity with Hydrocarbons and Small Molecules. *J. Am. Chem. Soc.* **1989**, *111*, 75−85.

(5) Buckner, S. W.; MacMahon, T. J.; Byrd, G. D.; Freiser, B. S. Gas-phase Reactions of Nb^+ and Ta^+ with Alkanes and Alkenes. C-H Bond Activation and Ligand-coupling Mechanisms. *Inorg. Chem.* **1989**, *28*, 3511−3518.

(6) Irikura, K. K.; Beauchamp, J. L. Methane Oligomerization in the Gas Phase by Third-row Transition-metal Ions. *J. Am. Chem. Soc.* **1991**, *113*, 2769−2770.

(7) Irikura, K. K.; Beauchamp, J. L. Electronic Structure Considerations for Methane Activation by Third-Row Transition-Metal Ions. *J. Phys. Chem.* **1991**, *95*, 8344−8351.

(8) Aschi, M.; Brönstrup, M.; Diefenbach, M.; Harvey, J. N.; Schröder, D.; Schwarz, H. A Gas-Phase Model for the Pt^+-Catalyzed Coupling of Methane and Ammonia. *Angew. Chem., Int. Ed.* **1998**, *37*, 829−832.

(9) Achatz, U.; Beyer, M.; Joos, S.; Fox, B. S.; Niedner-Schatteburg, G.; Bondybey, V. E. The Platinum Hydrido-Methyl Complex: A Frozen Reaction Intermediate? *J. Phys. Chem. A* **1999**, *103*, 8200−8206.

(10) Diefenbach, M.; Brönstrup, M.; Aschi, M.; Schröder, D.; Schwarz, H. HCN Synthesis from Methane and Ammonia: Mechanisms of Pt^+-Mediated C-N Coupling. *J. Am. Chem. Soc.* **1999**, *121*, 10614−10625.

(11) Rakowitz, F.; Marian, C. M.; Schimmelpfennig, B. Ground and Excited States of $PtCH_2^+$: Assessment of the No-pair Douglas-Kroll Ab Initio Model Potential Method. *Phys. Chem. Chem. Phys.* **2000**, *2*, 2481−2488.

(12) (a) Roithová, J.; Schröder, D. Selective Activation of Alkanes by Gas-Phase Metal Ions. *Chem. Rev.* **2010**, *110*, 1170−1211. (b) Schlangen, M.; Schwarz, H. *Catal. Lett.* **2012**, *142*, 1265.

(13) Zhang, X. G.; Liyanage, R.; Armentrout, P. B. Potential Energy Surface for Activation of Methane by Pt^+: A Combined Guided Ion Beam and DFT Study. *J. Am. Chem. Soc.* **2001**, *123*, 5563−5575.

(14) Armentrout, P. B.; Shin, S.; Liyanage, R. Guided-ion Beam and Theoretical Study of the Potential Energy Surface for Activation of Methane by W^+. *J. Phys. Chem. A.* **2006**, *110*, 1242−1260.

(15) Li, F. X.; Zhang, X. G.; Armentrout, P. B. The Most Reactive Third-row Transition Metal: Guided Ion Beam and Theoretical Studies of the Activation of Methane by Ir^+. *Int. J. Mass Spectrom.* **2006**, *255*−*256*, 279−300.

(16) Parke, L. G.; Hinton, C. S.; Armentrout, P. B. Experimental and Theoretical Studies of the Activation of Methane by Ta. *J. Phys. Chem. C* **2007**, *111*, 17773−17787.

(17) Irikura, K. K.; Goddard, W. A., III Energetics of Third-Row Transition Metal Methylidene Ions MCH_2^+ (M = La, Hf, Ta, W, Re, Os, Ir, Pt, Au). *J. Am. Chem. Soc.* **1994**, *116*, 8733−8740.

(18) Simon, A.; Lemaire, J.; Boissel, P.; Maître, P. Competition Between Agostic WCH_2^+ and $HWCH^+$: A Joint Experimental and Theoretical Study. *J. Chem. Phys.* **2001**, *115*, 2510−2518.

(19) Schrock, R. R. Alkylidene Complexes of Niobium and Tantalum. *Acc. Chem. Res.* **1979**, *12*, 98-104

(20) Goddard, R. J.; Hoffmann, R.; Jemmis, E. D. Unusual Metal-Carbon-Hydrogen Angles, Carbon-Hydrogen Bond Activation, and α-Hydrogen Abstraction in Transition-Metal Carbene Complexes. *J. Am. Chem. Soc.* **1980**, *102*, 7667−7676.

(21) Brookhart, M.; Green, M. L. H. Carbon-Hydrogen−Transition Metal Bonds. *J. Organomet. Chem.* **1983**, *250*, 395−408.
(22) Scherer, W.; McGrady, G. S. Agostic Interactions in d^0 Metal Alkyl Complexes. *Angew. Chem., Int. Ed.* **2004**, *43*, 1782−1806.
(23) Brookhart, M.; Green, M. L. H.; Parkin, G. Agostic Interactions in Transition Metal Compounds. *Proc. Natl. Acad. Sci.* **2007**, *104*, 6908−6914.
(24) Oomens, J.; Sartakov, B. G.; Meijer, G.; von Helden, G. Gas-phase Infrared Multiple Photon Dissociation Spectroscopy of Mass-Selected Molecular Ions. *Int. J. Mass Spectrom.* **2006**, *254*, 1−19.
(25) Asmis, K. R.; Sauer, J. Mass-Selective Vibrational Spectroscopy of Vanadium Oxide Cluster Ions. *Mass Spectrom. Rev.* **2007**, *26*, 542−562.
(26) Polfer, N. C.; Oomens, J. Vibrational Spectroscopy of Bare and Solvated Ionic Complexes of Biological Relevance. *Mass Spectrom. Rev.* **2009**, *28*, 468−494.
(27) Polfer, N. C. Infrared Multiple Photon Dissociation Spectroscopy of Trapped Ions. *Chem. Soc. Rev.* **2011**, *40*, 2211−2221.
(28) Black, J. G.; Yablonovitch, E.; Bloembergen, N.; Mukamel, S. Collisionless Multiphoton Dissociation of SF_6: A Statistical Thermodynamic Process. *Phys. Rev. Lett.* **1977**, *38*, 1131−1134.
(29) Grant, E.; Schulz, P.; Sudbo, A. S.; Shen, Y.; Lee, Y. T. Is Multiphoton Dissociation of Molecules a Statistical Thermal Process? *Phys. Rev. Lett.* **1978**, *40*, 115−118.
(30) Lehmann, K. K.; Scoles, G.; Pate, B. H. Intramolecular Dynamics from Eigenstate-Resolved Infrared-Spectra. *Annu. Rev. Phys. Chem.* **1994**, *45*, 241−274.
(31) Beil, A.; Luckhaus, D.; Quack, M.; Stohner, J. Intramolecular Vibrational Redistribution and Unimolecular Reaction: Concepts and New Results on the Femtosecond Dynamics and Statistics in CHBrClF. *Ber. Bunsen Phys. Chem.* **1997**, *101*, 311−328.
(32) Pivonka, N. L.; Kaposta, C.; von Helden, G.; Meijer, G.; Wöste, L.; Neumark, D. M.; Asmis, K. R. Gas Phase Infrared Spectroscopy of Cluster Anions as a Function of Size: The Effect of Solvation on Hydrogen-Bonding in $Br^-(HBr)_{1,2,3}$ Clusters. *J. Chem. Phys.* **2002**, *117*, 6493−6499.
(33) Pivonka, N. L.; Kaposta, C.; Brümmer, M.; von Helden, G.; Meijer, G.; Wöste, L.; Neumark, D. M.; Asmis, K. R. Probing a Strong Hydrogen Bond with Infrared Spectroscopy: Vibrational Predissociation of $BrHBr^-Ar$. *J. Chem. Phys.* **2003**, *118*, 5275−5278.
(34) Letokhov, V. S.; Ryabov, E. A.; Tumanov, O. A. Luminiscence of a Molecular Gas under the Action of CO_2 Laser Pulses. *Sov. Phys. JETP* **1973**, *36*, 1069−1073.
(35) Campbell, J. D.; Hancock, G.; Halpern, J. B.; Welge, K. H. Off Resonant Dissociation of NH_3 to Ground State Fragments by Pulsed CO_2 Laser Radiation. *Chem. Phys. Lett.* **1976**, *44*, 404−410.
(36) Bakker, J. M.; Lapoutre, V. J. F.; Redlich, B.; Oomens, J.; Sartakov, B. G.; Fielicke, A.; von Helden, G.; Meijer, G.; van der Meer, A. F. G. Intensity-resolved IR Multiple Photon Ionization and Fragmentation of C_{60}. *J. Chem. Phys.* **2010**, *132*, 074305.
(37) Haertelt, M.; Lapoutre, V. J. F.; Bakker, J. M.; Redlich, B.; Harding, D. J.; Fielicke, A.; Meijer, G. Structure Determination of Anionic Metal Clusters via Infrared Resonance Enhanced Multiple Photon Electron Detachment Spectroscopy. *J. Phys. Chem. Lett.* **2011**, *2*, 1720−1724.
(38) Dietz, T. G.; Duncan, M. A.; Powers, D. E.; Smalley, R. E. Laser Production of Supersonic Metal Cluster Beams. *J. Chem. Phys.* **1981**, *74*, 6511−6512.
(39) Bondybey, V. E.; English, J. H. Laser Induced Fluorescence of Metal Clusters Produced by Laser Vaporization: Gas Phase Spectrum of Pb_2. *J. Chem. Phys.* **1981**, *74*, 6978−6979.
(40) Duncan, M. A. Laser Vaporization Cluster Sources. *Rev. Sci. Instrum.* **2012**, *83*, 041101.
(41) Koszinowski, K.; Schröder, D.; Schwarz, H. Reactions of Platinum-Carbene Clusters $Pt_nCH_2^+$ (n = 1−5) with O_2, CH_4, NH_3, and H_2O: Coupling Processes versus Carbide Formation. *Organometallics* **2003**, *22*, 3809−3819.
(42) Lemaire, J.; Boissel, P.; Heninger, M.; Mauclaire, G.; Bellec, G.; Mestdagh, H.; Le Caer, S.; Ortega, J.; Glotin, F.; Maître, P. Gas Phase Infrared Spectroscopy of Selectively Prepared Ions. *Phys. Rev. Lett.* **2002**, *89*, 273002.
(43) Bakker, J. M.; Besson, T.; Lemaire, J.; Scuderi, D.; Maître, P. Gas-Phase Structure of a π-allyl-Palladium Complex: Efficient Infrared Spectroscopy in a 7T Fourier Transform Mass Spectrometer. *J. Phys. Chem. A* **2007**, *111*, 13415.
(44) Heinemann, C.; Wesendrup, R.; Schwarz, H. Pt^+-mediated Activation of Methane: Theory and Experiment. *Chem. Phys. Lett.* **1995**, *239*, 75−83.
(45) Becke, A. D. Density-Functional Thermochemistry. III. The Role of Exact Exchange. *J. Chem. Phys.* **1993**, *98*, 5648−5652.
(46) Lee, C.; Yang, W.; Parr, R. G. Development of the Colle-Salvetti Correlation-Energy Formula into a Functional of the Electron Density. *Phys. Rev. B* **1988**, *37*, 785−789.
(47) Rappoport, D.; Furche, F. Property-Optimized Gaussian Basis Sets for Molecular Response Calculations. *J. Chem. Phys.* **2010**, *133*, 134105.
(48) Andrae, D.; Häußermann, U.; Dolg, M.; Stoll, H.; Preuß, H. Energy-adjusted Ab Initio Pseudopotentials for the Second and Third Row Transition Elements. *Theor. Chem. Acc.* **1990**, *77*, 123−141.
(49) Frisch, M. J.; et al. *Gaussian 03*, Revision C.02; Gaussian, Inc.: Wallingford, CT, 2004.
(50) Scurlock, C. T.; Pullins, S. H.; Reddic, J. E.; Duncan, M. A. Photodissociation Spectroscopy of Ca^+-H_2O and Ca^+-D_2O. *J. Chem. Phys.* **1996**, *104*, 4591−4599.
(51) von Helden, G.; Holleman, I.; Knippels, G. M. H.; van der Meer, A. F. G.; Meijer, G. Infrared Resonance Enhanced Multiphoton Ionization of Fullerenes. *Phys. Rev. Lett.* **1997**, *79*, 5234−5237.
(52) Calvo, F.; Parneix, P. Amplification of Anharmonicities in Multiphoton Vibrational Action Spectra. *ChemPhysChem.* **2012**, *13*, 212−220.
(53) Perry, J. K.; Ohanessian, G.; Goddard, W. A., III Mechanism and Energetics for Dehydrogenation of Methane by Gaseous Iridium Ions. *Organometallics* **1994**, *13*, 1870−1877.
(54) Musaev, D. G.; Morokuma, K. Ab-Initio Molecular-Orbital Study of Electronic and Geometrical Structures of MCH_2^+ Complex and its Reactivity with H_2, where M = Co, Rh, and Ir. *Isr. J. Chem.* **1993**, *33*, 307−316.
(55) Armentrout, M. M.; Li, F. X.; Armentrout, P. B. Is Spin Conserved in Heavy Metal Systems? Experimental and Theoretical Studies of the Reaction of Re^+ with Methane. *J. Phys. Chem. A* **2004**, *108*, 9660−9672.
(56) Zhang, G.; Li, S.; Jiang, Y. Dehydrogenation of Methane by Gas-Phase Os^+: A Density Functional Study. *Organometallics* **2003**, *22*, 3820−3830.
(57) Crabtree, R. H. *The Organometallic Chemistry of the Transition Metals*, 3rd ed.; John Wiley & Sons, Inc.: New York, 2001.
(58) Bakker, J. M.; Redlich, B.; van der Meer, A. F. G.; Oomens, J. Infrared Spectroscopy of Gas-phase Polycyclic Aromatic Hydrocarbon Cations in the 10−50 μm Spectral Range. *Astrophys. J.* **2011**, *741*, 74.